Available online at www.sciencedirect.com
SCIENCE DIRECT®
Journal of Magnetic Resonance 168 (2004) 97–102
JMR Journal of Magnetic Resonance
www.elsevier.com/locate/jmr

Frequency shifts in parametrically enhanced low-field MR detection

Daniel W. Sinkovits and Mark S. Conradi*

Department of Physics, Washington University, CB 1105, St. Louis, MO 63130-4899, USA

Received 23 October 2003; revised 27 January 2004

Abstract

A high-amplitude, high-frequency readout field has previously been proposed for use with low-field MR. Because the resulting modulation sidebands are at higher frequencies than the low-field steady precession, improved detection sensitivity results. However, if the ac readout field is inhomogeneous, it will necessarily have transverse components resulting in frequency shifts and broadening of the MR signal. Numerical solutions of Bloch's equations are compared to the Bloch–Siegert result to assess the size of the frequency shifts. A formula is derived by the average Hamiltonian method and provides an excellent fit to the numerically obtained shifts.

1. Introduction

The sensitivity of magnetic resonance is predicted [1] to vary as $B_0^{7/4}$, where B_0 is the static field strength. One power of B_0 results from the thermal equilibrium spin polarization, in the nearly always relevant high-temperature approximation [2]. The remaining $B_0^{3/4}$ dependence results from the use of magnetic induction to generate a voltage in the receiving coil proportional to the time derivative of the magnetization. The exact dependence of this term depends on how the coil Q varies with frequency f_0, where $f_0 = \gamma B_0/2\pi$.

Despite the low sensitivity, there are many applications and potential applications for low-field NMR [3,4]. These include oil-well logging [5], mapping of the earth's magnetic field, and detection of water buried in a structure such as a concrete bridge. In all of these, it is impractical to immerse the entire "sample" in a uniform static field of high strength. Another application is low-field MRI [6], where the use of a homogeneous but weak field B_0 essentially eliminates effects of the sample's magnetic susceptibility variations [7] and substantially reduces the magnet's cost.

One route to higher sensitivity in low-field MR is the use of prepolarized spins. This may take the form of Overhauser enhancement of nuclear polarization [8] by saturation of dissolved electron spins. Optically pumped (hyperpolarized) gases can be imaged at low fields with reasonable sensitivity [9,10]. Another technique uses a prepolarizing field pulse of duration one or two times T_1 to align the spins for subsequent low-field MR or MRI [6,11,12]. We note that the first observation of NMR in the earth's field used a prepolarizing pulsed field [13]. All these methods increase the nuclear spin polarization above the equilibrium value in the low field.

In low field, the detection sensitivity still suffers because of the low-readout frequency, $f_0 = \gamma B_0/2\pi$. Macovski and Conolly [11] proposed using an additional ac readout field of frequency f, parallel to B_0, to increase the detection frequency and, as a result, the sensitivity. We consider here the most practical scheme suggested, using a sinusoidal field B_1,

$$B_{1(t)} = B_{1p}\cos 2\pi f t, \tag{1}$$

where B_{1p} is the peak amplitude. We note this field B_1 is a modulation field parallel to B_0 and is distinct from any possible third field intended to nutate the spins. Spin magnetization $\mathbf{M}$ will precess about the z-axis under the combined effects of B_0 and $B_{1(t)}$. For spins initially along the x-axis ($\phi = 0$ at $t = 0$)

$$\phi_{(t)} = \int_{t'=0}^{t} \gamma(B_0 + B_{1(t')})\mathrm{d}t' = \gamma B_0 t + \left(\frac{\gamma B_{1p}}{2\pi f}\right)\sin 2\pi f t. \tag{2}$$

* Corresponding author. Fax: 1-314-935-6219.
E-mail address: msc@wuphys.wustl.edu (M.S. Conradi).

1090-7807/$ - see front matter © 2004 Elsevier Inc. All rights reserved.
doi:10.1016/j.jmr.2004.02.002

We note that the problem is described by three frequencies: the static precession frequency $f_0 = \gamma B_0/2\pi$, the frequency f of the ac field B_1, and $f_1 \equiv \gamma B_{1p}/2\pi$ which is the peak amplitude of B_1 in spin-frequency units. Eq. (2) describes [14] frequency modulation (FM) with a modulation index m

$$m \equiv \gamma B_{1p}/2\pi f = f_1/f. \tag{3}$$

The MR signal is $\exp(i\phi_{(t)})$ and can be expressed as a frequency spectrum consisting of a centerband at f_0 and sidebands at $f_0 \pm nf$ where n is integer [14–16]. For $f \gg f_0$, all of these sidebands are at higher frequencies (in magnitude) than f_0, offering the possibility of increased detection sensitivity.

The spin magnetization **M**, oscillating back and forth about B_1 while it slowly precesses about B_0, is sketched in Fig. 1A. There the field B_1 is parallel to B_0 and the z-axis and $f = 10f_0$; the sketch presents one full cycle of precession at f_0. The phase ϕ is taken from Eq. (2). A pick-up coil along the y-axis will detect a voltage proportional to dM_y/dt, as displayed in Fig. 1B. There, components near the pump frequency f appear, with beating evident between the $n = 1$ and -1 sidebands. A weak component is present at the unmodulated frequency f_0 and $n = \pm 2$ sidebands at frequencies near $2f$ are evident near the nodes in the beat pattern.

We consider use of the first sidebands only ($n = \pm 1$) at frequencies $f - f_0$ and $f + f_0$. Their amplitudes are maximized by adjusting the amplitude B_{1p} to yield [11,14] $m = 1.85$; this corresponds to a peak-to-peak rotation of the magnetization **M** through an angle of $2m$, somewhat greater than π radians. The sidebands can be detected in a pick-up coil, amplified, and heterodyned against a reference at f, returning a signal at the difference frequency, f_0. Thus the use of the ac field does not shift or broaden the NMR signal; the frequency of the returned signal does not depend on the frequency or amplitude of the ac field. Because the field B_1 acts on the frequency (a "parameter" of the spins) and does not drive (nutate) the spins, we refer to this method as parametrically enhanced MR detection. We note that any leakage of the B_1 ac field at frequency f into the detection pick-up coil produces a dc output from the heterodyne mixer and is easily removed, putting aside issues of dynamic range. Thus, the weak field B_0 plays an important role, separating the modulation sideband signals from the pump leakage by their frequencies.

The potential advantage of parametrically enhanced MR detection, compared to simply using a larger static field B_0, is that the ac pumping field B_1 need not be spatially uniform (while the homogeneity of B_0 directly determines the linewidth). A variation in B_{1p} away from its optimum value corresponding to $m = 1.85$ simply results in a slight sensitivity decrease, without frequency broadening. In general, it is much more practical to provide a large but inhomogeneous ac field B_1 with a small and uniform B_0 than to provide a large and uniform B_0. A homogeneous pumping field would be synonymous with much more required power, because it would involve a physically larger coil with a larger volume pumping field. We note that parametrically enhanced detection has not been implemented; in MRI of humans, a large-amplitude high-frequency pump field may dissipate excessive heat in the subject. We note that the power dissipation will vary as f^4 for a fixed modulation index m, because the amplitude B_{1p} and f both

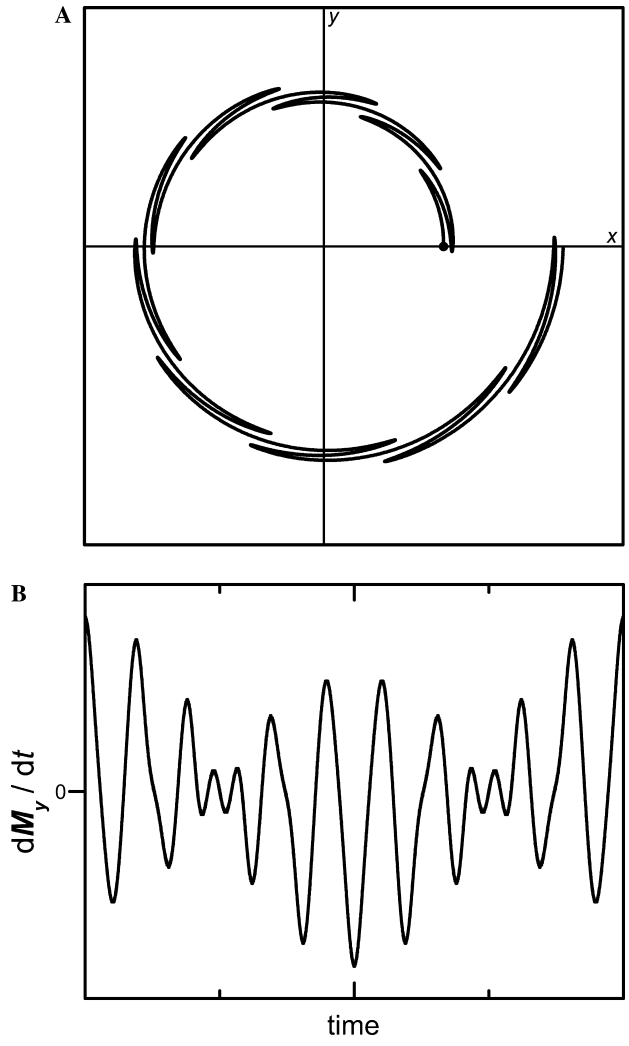

Fig. 1. (A) Spin magnetization, represented as a vector-dot, precessing about z-axis under combined effects of a weak static field B_0 (with $f_0 = \gamma B_0/2\pi$) and a strong ac field B_1 at frequency f, with $f = 10f_0$. Both B_0 and B_1 are along the z-axis. The magnetization starts along the x-axis; the length of the vector is increased with time for display purposes. The peak amplitude of B_1 corresponds to modulation index $m = 0.7$; m is the peak phase modulation. (B) Signal voltage induced in detection coil along y-axis, proportional to dM_y/dt. As in (A), one cycle of precession about B_0 is shown, corresponding to 10 cycles of modulation frequency f. The left-hand edge is at the initial time (dot in (A)). In addition to the main components at $f \pm f_0$ ($n = \pm 1$ sidebands) with the evident beat pattern, some signal at f_0 is present. Signal at $\approx 2f$ is apparent near the nodes in the beat pattern.

scale as f and dissipated power is quadratic in the induced currents. Thus, concerns of power dissipated into the subject will limit the frequency (and sensitivity improvement) of parametrically enhanced MR in humans.

The above remarks apply for the case of B_1 directed along the z-axis, parallel to B_0. However, if B_1 is not spatially uniform, it cannot be everywhere parallel to B_0: Maxwell's equations dictate [17] that non-uniform magnetic fields have field lines that converge and diverge *by changing direction*. Now, it is well-known that off-resonance rotating and oscillating fields with components perpendicular to B_0 generate Bloch–Siegert frequency shifts [8,18]. In the present context of an inhomogeneous pumping field B_1, such shifts will generate line broadening of the NMR signal. This broadening will reduce the signal-to-noise (S/N) and may negate the expected sensitivity increase. Thus, experimental success of parametrically enhanced NMR detection requires a compromise: if the B_1 pump field is insufficiently homogeneous, line broadening and decreased S/N will occur; if B_1 is more than adequately uniform, there will be no further decrease in linewidth and no further increase in S/N, but there will be a large increase in the power required to drive the pump field-coil. We note this power is expected to be substantial. This is the issue addressed here—how large are the frequency shifts in parametrically enhanced MR detection? The question is addressed by numerical solutions of Bloch's free-precession equations and comparison to the Bloch–Siegert result. A nearly exact result for $f \gg f_0$ is derived.

2. Method

Bloch's free-precession equations, $\dot{\mathbf{M}} = \gamma(\mathbf{M} \times \mathbf{B})$ [2,8] were integrated using the program Matlab on a personal computer. The magnetic field was taken to be the sum of B_0 in the z-direction and the oscillating field B_1 of Eq. (1) in the x–z plane, at angle θ to the z-axis. Exactly one cycle of the oscillating field B_1 was divided into 1000 time steps for Runge–Kutta integration; we verified that use of more steps did not change the results. The integration yielded an output matrix specifying the spin magnetization $\mathbf{M}$ after one cycle, in terms of the initial magnetization $\mathbf{M}_0$. The matrix is a rotation operator, because it is the result of many (e.g., 1000) smaller rotations in sequence. The rotation axis of the operator and its rotation angle α (in radians) were found. Thus, the overall frequency f_s of the spin motion under the combined effects of B_0 and B_1 is

$$f_s = \alpha/(2\pi/f). \tag{4}$$

The results are reported in terms of the frequency shift $\Delta f \equiv f_s - f_0$. We note the modulation index m is $m = f_1/f$.

The numerical results are compared to the well-known Bloch–Siegert result. For a rotating field at frequency f with magnitude f_1, the Bloch–Siegert frequency shift Δf away from the free precession frequency f_0 is in general [8,18]

$$\Delta f = \frac{f_1^2}{2(f_0 - f)}. \tag{5}$$

This result holds for weak rotating fields, $f_1 \ll |f_0 - f|$. In the present problem, we treat the oscillating field in the x-direction as two counter-rotating fields at frequencies f and $-f$, each with magnitude $f_1 \sin\theta/2$. Thus the sum of the shifts from each rotating field is

$$\Delta f = \frac{f_1^2 \sin^2\theta}{8}\left(\frac{1}{f_0 - f} + \frac{1}{f_0 + f}\right). \tag{6}$$

To obtain a useful sensitivity enhancement one must have $f \gg f_0$, so the two terms in parentheses have opposite signs. Adding, one obtains

$$\Delta f = \frac{f_1^2 f_0 \sin^2\theta}{4(f_0^2 - f^2)} \cong \frac{-f_1^2 f_0 \sin^2\theta}{4f^2} = \frac{-m^2 f_0 \sin^2\theta}{4}, \tag{7}$$

this is the result for simply adding the Bloch–Siegert shifts from the two rotating fields. We note that, for large angles θ and modulation indices $m \gtrsim 1$, the assumption used in obtaining Eq. (5) (that the RF field strength is small compared to the resonance offset) is not valid.

3. Results

Numerical results for the case of B_1 not parallel to B_0 appear in Fig. 2. The parameters were chosen to be relevant to detection in the earth's field ($f_0 = 2000$ Hz) with a substantially larger pump frequency ($f = 100$ kHz) to yield a significant boost in detection sensitivity. The peak amplitude was selected to yield a large modulation index for good sensitivity ($f_1 = 110$ kHz, so $m = 1.1$). In Fig. 2A, the shift Δf is reported as a function of the tilt angle θ of B_1. In agreement with Eq. (7), Δf is negative and varies nearly as $\sin^2\theta$. In Fig. 2B, the shift varies nearly as f_1^2, in agreement with formula (7).

In both Figs. 2A and B, the agreement with the prediction is good for small shifts ($|\Delta f| < 100$ Hz), but the numerical result becomes smaller in magnitude than Eq. (7) result for larger shifts. In Fig. 2C, the shift Δf is found to vary linearly with f_0, in agreement with the prediction of Eq. (7). But the magnitude of the slope is smaller than predicted, similar to the deviations in Figs. 2A and B.

For the values in Fig. 2A, which would yield a very substantial factor of 50 (that is, f/f_0) increase in detection frequency, the calculated frequency shifts are reasonably approximated by Eq. (7). The shift remains

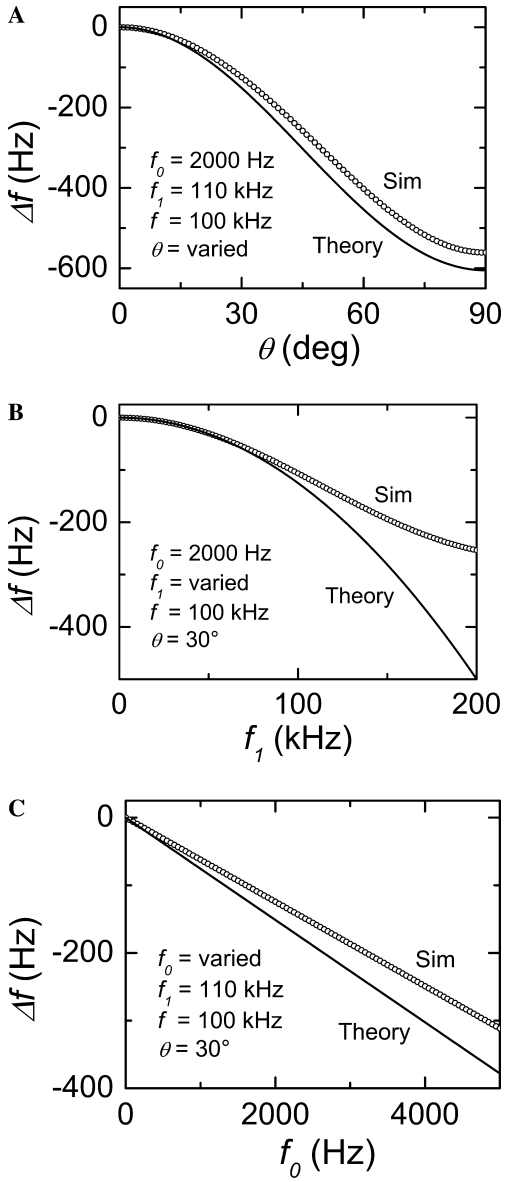

Fig. 2. Frequency shift $\Delta f = f_s - f_0$ resulting from components of the oscillating field B_1 perpendicular to the static field B_0. In each case, "Theory" reports the predictions of Eq. (7) and "Sim" reports the results of numerical simulation (integration) of Bloch's precession equations. (A) Δf as function of tilt angle θ, compared to $\sin^2\theta$ prediction. (B) Δf as function of oscillating field amplitude f_1; the theory prediction varies as f_1^2. (C) Δf variation with f_0; here the theory prediction is linear.

smaller than 100 Hz (5% of f_0) for all tilt angles less than 27° and smaller than 25 Hz (1.25%) for angles below 13°. Thus, a reasonably inhomogeneous pump field can be used, depending on the application (low-field spectroscopy, detection of buried water, etc.). We note that the same coil could be used to provide a prepolarizing field pulse and later provide the ac parametric pump field; in neither case is field uniformity crucial.

An interesting issue is the extent to which the longitudinal component of the oscillating field B_1 changes the

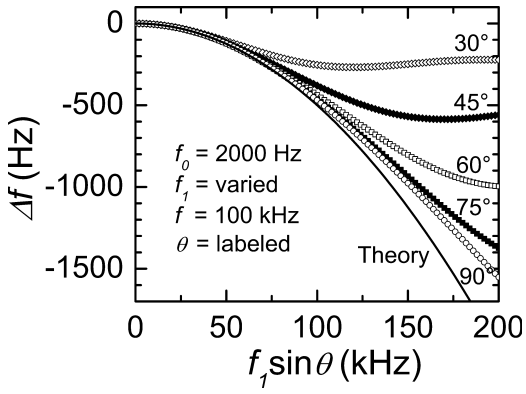

Fig. 3. Frequency shift Δf from numerical integration of Bloch's equations as a function of the transverse field peak amplitude $f_1 \sin\theta$, for five values of tilt angle θ. At small θ, the longitudinal oscillating field $f_1 \cos\theta$ becomes large and suppresses the shift. The curve marked "Theory" is the result of Eq. (7).

frequency shift arising from the transverse components. The shifts for five tilt angles θ are compared in Fig. 3, all with the same magnitudes of transverse field components, $f_1 \sin\theta$. In one case $\theta = 90°$, so the longitudinal component is zero; at the other extreme, $\theta = 30°$ so the longitudinal component is $\sqrt{3}$ times as large as the transverse. At small magnitudes of transverse oscillating fields, the shifts are all nearly the same, demonstrating that the oscillating longitudinal field does not much modify the frequency shift. But at small angles θ and at large values of the transverse field $f_1 \sin\theta$, that is $f_1 \sin\theta \gtrsim f$, the strong longitudinal field reduces the magnitude of the frequency shift. Qualitatively, the rapid precession about the strong longitudinal component of B_1 provides some motional averaging (reduction) of the effects of the weaker transverse fields.

Several discussions of Bloch–Siegert frequency shifts have treated fields of amplitude not small compared to the frequency offsets [19–21]. As derived in Appendix A, for $f \gg f_0$ the spin frequency f_s taken from Eq. (4) is given by

$$f_s = f_0\sqrt{\cos^2\theta + \sin^2\theta J^2_{0(f_1/f)}}, \tag{8}$$

where J_0 is the zeroth order Bessel function. This formula correctly yields $f_s = f_0$ in the case $f_1 = 0$, as $J_{0(0)}$ is then unity. An interesting limit (but not relevant to practical use of parametrically enhanced detection) is extremely large modulation indices, $m = f_1/f \gg 1$. Since J_0 goes to zero in this limit, f_s becomes $f_0 \cos\theta$. The implication is clear—only the component of B_0 along the (tilted) oscillating field B_1 is important in this limit. In the limit of $m = f_1/f \ll 1$, the Bessel function and square root can be expanded to yield the same result as approximation (7).

Numerical results for spin precession frequency f_s are presented in Fig. 4 over a wide range of modulation indices m and tilt angles θ. The predictions of Eq. (8) are

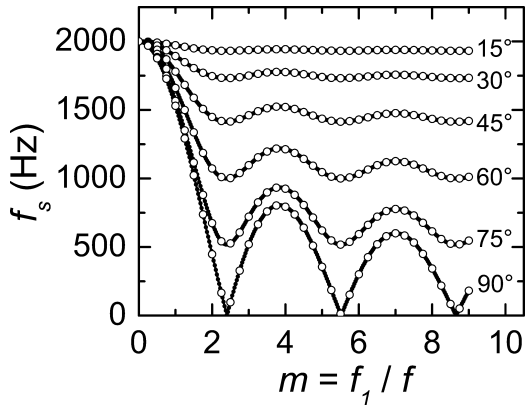

Fig. 4. Spin precession frequency f_s as a function of the modulation index $m = f_1/f$ for six values of the tilt angle θ. For all, f_0 is 2000 Hz and the frequency of the tilted field is 100 kHz. The solid black curves are from numerical (exact) calculations; the open circles are from formula (8).

also displayed and show excellent agreement, with no adjustable parameters. Thus, formula (8) is applicable to much larger values of m and tilt angle θ than is the simpler approximation (7). Is Eq. (8) exact? No; when f_0 is no longer small compared to f, substantial differences between (8) and the numerical results appear (data not shown). Indeed, the derivation of Eq. (8) by the average Hamiltonian method relies on $f \gg f_0$. But parametrically enhanced NMR with useful sensitivity increase is limited to $f \gg f_0$, where formula (8) works exceedingly well.

4. Conclusions

There are many MR applications in which it is impractical to provide an intense and uniform static field throughout the sample. Low-field MR requires only a weak uniform field, but the sensitivity is lower at low-field strengths. Dynamically polarized spins or the use of a prepolarizing field pulse can increase the sensitivity of low-field MR. Further, use of a high-amplitude, high-frequency readout field (parametrically enhanced detection) can increase the frequency of the spin signal and the detection sensitivity.

Transverse components will result from inhomogeneity of the ac readout field and will generate frequency shifts and broadenings, leading to reduced detection sensitivity. Such shifts have been calculated here by numerical integration of the free-precession equations of motion for spin magnetization. The frequency shift is found to substantially agree with a simple prediction based on the Bloch–Siegert effect. Specifically, the shift is to lower frequency, varies with the field tilt-angle θ nearly as $\sin^2\theta$, varies approximately as the square of the field amplitude f_1, and is linearly proportional to the static precession frequency f_0. In general, the naïve formula based on Bloch–Siegert shifts from two counter-rotating field components overestimates the actual shift magnitudes. A simple formula is derived that provides excellent agreement with no adjustable parameters to the numerical (exact) results.

For values of the parameters describing a typical application (earth's field NMR) with a substantial boost in detection frequency (factor of 50), the shifts are modest (<5% of f_0) provided the tilt angle remains below 27°.

Acknowledgments

The authors acknowledge support through NSF Grant DMR-9987888 and NIH Grant R01 HL70037.

Appendix A. Average hamiltonian derivation of spin frequency

Here we choose the z-axis along the oscillating field $\mathbf{B}_1$ and the x-axis perpendicular to z in the $\mathbf{B}_0 - \mathbf{B}_1$ plane. The instantaneous classical Hamiltonian is $\mathcal{H} = -\mathbf{M}\cdot\mathbf{B}$, which becomes

$$\mathcal{H} = -M_z(B_{1p}\cos\omega t + B_0\cos\theta) - M_x B_0 \sin\theta, \tag{A.1}$$

where $\mathbf{M}$ is the vector spin magnetization and M_z and M_x are components of $\mathbf{M}$; $\omega \equiv 2\pi f$. To lowest order in the average Hamiltonian method, the quantities in (A.1) are to be evaluated after time-averaging over a complete cycle of the oscillatory field. In this averaging, only the motion driven by the oscillating field is considered. We note that the average Hamiltonian method depends on the precession angle about B_0 being small during one period of the oscillating pump field, so $f_0 \ll f$. Thus, M_z is constant and M_x will be partially averaged by precession about $\mathbf{B}_1$ to become $\overline{M}_x$. Also the average of $\cos\omega t$ is zero, so the average Hamiltonian becomes

$$\overline{\mathcal{H}} = -M_z B_0\cos\theta - \overline{M}_x B_0 \sin\theta. \tag{A.2}$$

To find $\overline{M}_x$ we write

$$M_{+(t)} = M_{+0}\mathrm{e}^{\mathrm{i}\phi} = M_{+0}\mathrm{e}^{\mathrm{i}m\sin\omega t}, \tag{A.3}$$

following Eq. (2). The standard Bessel expansion for the exponential yields for the complex magnetization $M_+ \equiv M_x + \mathrm{i}M_y$,

$$M_{+(t)} = M_{+0}\sum_n J_{n(m)}\mathrm{e}^{\mathrm{i}n\omega t}, \tag{A.4}$$

where n runs over all integers, $-\infty$ to ∞. The time average of the above yields only the $n = 0$ term

$$\overline{M}_+ = M_{+0}J_{0(m)}, \tag{A.5}$$

the real part of which is

$$\overline{M}_x = M_{x_0}J_{0(m)}. \tag{A.6}$$

Thus the average Hamiltonian of (A.2) becomes

$$\overline{\mathcal{H}} = -M_z B_0 \cos\theta - M_{x_0} B_0 \sin\theta J_{0(m)}, \tag{A.7}$$

this is simply the Hamiltonian of magnetization **M** in a hypothetical field **B′**

$$\mathbf{B}' = \hat{z}(B_0 \cos\theta) + \hat{x}(B_0 \sin\theta J_{0(m)}). \tag{A.8}$$

Thus the spin precession frequency f_s is $\gamma|B'|/2\pi$ or

$$f_s = (\gamma/2\pi)B_0\sqrt{\cos^2\theta + \sin^2\theta J_{0(m)}^2}, \tag{A.9}$$

by Pythagoras' theorem; this result appears in the text as Eq. (8).

References

[1] D.I. Hoult, R.E. Richards, The signal-to-noise ratio of the nuclear magnetic resonance experiment, J. Magn. Reson. 24 (1976) 71–85.

[2] C.P. Slichter, Principles of Magnetic Resonance, Springer, New York, 1996, pp. 11–39.

[3] B. Blümich, NMR Imaging of Materials, Oxford University Press, Oxford, 2000, pp. 401–423.

[4] G.-J. Béné, High resolution NMR spectroscopy in the terrestrial magnetic field range, in: R. Blinc (Ed.), Magnetic Resonance and Relaxation, North-Holland, Amsterdam, 1967, pp. 903–916.

[5] R.L. Kleinberg, A. Sezginer, D.D. Griffin, M. Fukuhara, Novel NMR apparatus for investigating an external ample, J. Magn. Reson. 97 (1992) 466–485.

[6] P. Morgan, S. Conolly, G. Scott, A. Macovski, A readout magnet for prepolarized MRI, Magn. Reson. Med. 36 (1996) 527–536.

[7] D.A. Yablonskiy, Quantitation of intrinsic magnetic susceptibility-related effects in a tissue matrix. Phantom study, Magn. Reson. Med 39 (1998) 417–428.

[8] A. Abragam, The Principles of Nuclear Magnetism, Oxford University Press, London, 1961.

[9] E. Durand, G. Guillot, L. Darrasse, G. Tastevin, P.J. Nacher, A. Vignaud, D. Vattolo, J. Bittoun, CPMG measurements and ultrafast imaging in human lungs with hyperpolarized helium-3 at low field (0.1 T), Magn. Reson. Med. 47 (2002) 75–81.

[10] C.P. Bidinosti, J. Choukeife, P.-J. Nacher, G. Tastevin, In vivo NMR of hyperpolarized ^{3}He in the human lung at very low magnetic fields, J. Magn. Reson. 162 (2003) 122–132.

[11] A. Macovski, S. Conolly, Novel approaches to low-cost MRI, Magn. Reson. Med. 30 (1993) 221–230.

[12] B.F. Melton, V.L. Pollak, Condition for adiabatic passage in the earth's field NMR technique, J. Magn. Reson. 158 (2002) 15–22.

[13] M. Packard, R. Varian, Free nuclear induction in the earth's magnetic field, Phys. Rev. 93 (1954) 941.

[14] F.E. Terman, Radio Engineers' Handbook, McGraw-Hill, New York, 1943, pp. 578–588.

[15] J.T. Arnold, M.E. Packard, Variations in absolute chemical shift of nuclear induction signals of hydroxyl groups of methyl and ethyl alcohol, J. Chem. Phys. 19 (1951) 1608–1609.

[16] W.A. Anderson, Applications of modulation techniques to high resolution NMR spectrometers, Rev. Sci. Instrum. 33 (1962) 1160–1166.

[17] D.J. Griffiths, Introduction to Electrodynamics, Prentice Hall, Upper Saddle River, NJ, 1999, pp. 202–254.

[18] F. Bloch, A. Siegert, Magnetic resonance for nonrotating fields, Phys. Rev. 57 (1940) 522–527.

[19] P. Hannaford, D.T. Pegg, G.W. Series, Analytical expressions for the Bloch–Siegert shift, J. Phys. B 6 (1973) L222–L225.

[20] D.T. Pegg, Misalignment effects in magnetic resonance, J. Phys. B 6 (1973) 241–245.

[21] D.T. Pegg, Semi-classical model of magnetic resonance in intense RF fields, J. Phys. B 6 (1973) 246–253.